

# FedMed-GAN: Federated Multi-Modal Unsupervised Brain Image Synthesis

Guoyang Xie<sup>1,2,†</sup>, Jinbao Wang<sup>2,5,†</sup>, Yawen Huang<sup>3,†</sup>, Yefeng Zheng<sup>3</sup>, Feng Zheng<sup>2</sup>, Jingkuang Song<sup>5</sup>,  
 Yaochu Jin<sup>1,4</sup>  
<sup>1</sup>NICE Group, University of Surrey  
<sup>2</sup>VIP Lab, Southern University of Science and Technology  
<sup>3</sup>Javis Lab, Tencent  
<sup>4</sup>Bielefeld University  
<sup>5</sup>University of Electronic Science and Technology of China  
 {guoyang.xie, yaochu.jin}@surrey.ac.uk,  
 {wangjb, zhengf}@sustech.edu.cn,  
 {yawenhuang, yefeng.zheng}@tencent.com,  
 jingkuan.song@gmail.com

## Abstract

*Utilizing the paired multi-modal neuroimaging data has been proved to be effective to investigate human cognitive activities and certain pathologies. However, it is not practical to obtain the full set of paired neuroimaging data centrally since the collection faces several constraints, e.g., high examination costs, long acquisition time, and even image corruption. In addition, most of the paired neuroimaging data are dispersed into different medical institutions and cannot group together for centralized training considering the privacy issues. Under the circumstance, there is a clear need to launch federated learning and facilitate the integration of other unpaired data from different hospitals or data owners. In this paper, we build up a new benchmark for federated multi-modal unsupervised brain image synthesis (termed as FedMed-GAN) to bridge the gap between federated learning and medical GAN. Moreover, based on the similarity of edge information across multi-modal neuroimaging data, we propose a novel edge loss to solve the generative mode collapse issue of FedMed-GAN and mitigate the performance drop resulting from differential privacy. Compared with the state-of-the-art method shown in our built benchmark, our novel edge loss could significantly speed up the generator convergence rate without sacrificing performance under different unpaired data distribution settings. Our code will be released on the website: <https://github.com/FedMed-Meta/FedMed-GAN>.*

## 1. Introduction

The majority of existing medical datasets [1, 30, 5], especially for neuroimaging data, are high-dimensional and heterogeneous. For instance, positron emission tomography (PET) and magnetic resonance imaging (MRI) are the imaging techniques to measure the information of organs and tissues for helping diagnosis or monitor treatment. These pair of multi-modal data provide more complementary information to investigate the certain pathologies and neurodegeneration. However, it is not feasible to acquire a full set of paired multi-modal neuroimaging data. There are two issues: 1) collecting multi-modal neuroimaging data is very costly, for example, a normal MRI can take more than one thousand dollars in New York; 2) many medical institutions cannot share their data which is restricted to the local hospital regulations, despite the identifiable information has been removed for protecting the privacy of patients. Even in multi-hospital collaborative research, they would undertake integrated analysis rather than sharing research data with other hospitals. Hence, data isolation and privacy concerns are the fundamental problems blocking a large-scale and multi-institute neuroimaging research.

Generative adversarial networks (GANs) [12] are state-of-the-art deep generative models, which have achieved huge success in image synthesis. GANs alternatively train two networks, in which the generator maps a random input vector into a high-dimensional space and the discriminator judges the outputted data from real ones. These two networks aim to defeat each other. The training objective of the generator is to create a “fake” content to confuse the discriminator, while the objective of the discriminator

---

<sup>†</sup>Equal contribution.

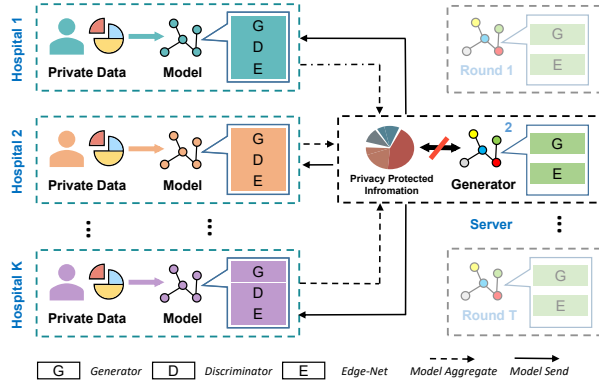


Figure 1. The pipeline of FedMed-GAN. Each client’s generators and edge-net are shared with the server and take part in federated learning process. But the discriminators of each client are not shared with each other.

is to improve distinguishable ability. GANs need a large amount of paired data for training, but most of the paired neuroimaging data are scattered in different hospitals. Due to privacy legislation, it is not feasible to aggregate the full set of paired neuroimages from various medical institutions.

Recently, a large amount of effort has been made to facilitate the availability of medical data without violating the privacy issue. Federated Learning (FL) is one of the popular approaches. FL is a decentralized approach where local clients train their local models without transmitting data to a central server, and the global model aggregates the gradients from clients [27]. In addition, FL with GANs has witnessed some pilot progress on image synthesis [7, 3]. For example, DP-FedAvg-GAN [3] trains GANs with the differential privacy-preserving algorithm, which clips the gradients to bound sensitivity and adds calibrated random noise to introduce stochasticity. Specifically, DP-FedAvg-GAN locates a discriminator for each client and a generator in the server. Each client updates its discriminator by using its own dataset and creates a fake image for the global generator. In this case, the generator is only exposed to the discriminator and never uses the real data. However, each client can only assess one domain data, which cannot fully leverage the existing training paradigm of GANs, especially for CycleGAN [37]. In addition, we also discover that DP-FedAvg-GAN may suffer from the generator mode collapse and slow down convergence rate in our built FedMed-GAN benchmark. The performance of DP-FedAvg-GAN is lower than the centralized training due to the differential privacy guarantee. Our method is inspired by RCF [26] and utilize the shared edge feature map across multi-modal neuroimages to guide the generator, which could largely mitigate the side effect brought by DP-FedAvg-GAN.

Our contributions can be summarized as follows:

- We build up a new benchmark for federated multi-

modal brain image synthesis (FedMed-GAN), which bridge the gap between federated learning and medical GAN. It significantly facilitates the development of medical GAN within differential privacy guarantee.

- We design a new edge loss to primarily prevent performance drop caused by differential privacy guarantee and also facilitate the convergence of FedMed-GAN.
- Our edge-guided federated training paradigm does not sacrifice the performance compared with centralized training.

## 2. Related Work

**Medical Image-to-Image Translation** Image-to-image translation (I2IT) aims to take images from one domain and translate them into images with a style (or characteristics) of another domain. It is first proposed in [18]. In specific, the Pix2Pix mode [18] demands the use of well-aligned paired images, which are not always available. CycleGAN [37] extends the generative framework to unpaired data and is capable of accomplishing unsupervised I2IT. Based on the cycle-consistency mode, many variants have been proposed. UNIT [24] makes use of two VAE encoders to map images from disparate domains into a common space. MUNIT [13] and DRIT [21, 22] disentangle content and style code to promote a variety of styles. Similarly, FUNIT [25] extends prior work in the area of few-shot scenarios and the model can be applied to a variety of domains with only a few examples in each. NICEGAN [9] suggests that the discriminator can be reused for encoding.

The existing medical imaging research, such as segmentation [29, 36, 34], registration [11, 10, 6] and synthesis [15, 16, 35], has demonstrated considerable prospects for both research and clinical analysis. However, the task of medical I2IT has not been paid much attention, despite the fact that it is a critical component of computer-assisted diagnosis. Huang *et al.* [17] proposed an unsupervised multivariate canonical CSCl<sub>4</sub>Net to perform cross-modal image synthesis considering both intra-modal and inter-modal heterogeneity. Kong *et al.* [20] introduced a new I2IT model called RegGAN, which converts the unsupervised I2IT task into a supervised I2IT with noisy labels. However, none of their work focuses on the privacy of medical data, bringing harmful effects of further deployment.

**Federated Learning** Federated learning, as a privacy-preserving decentralized learning strategy, allows clients train their own models without communicating data to a central server, and the global model is updated by aggregating client updates. FedAvg [28] combines local stochastic gradient descent (SGD) on each client with a server that performs model averaging. Yurochkin *et al.* [33] developed a Bayesian non-parametric framework for federated learning with neural networks. FedProx [23] provides a gener-

alized and re-parametrized FedAvg that addresses the challenges of heterogeneity both theoretically and empirically. FedMA [32] constructs the shared global model in a layer-wise manner by matching and averaging hidden elements with similar feature extraction signatures.

Incorporating the generative adversarial framework into the federated learning is challenging, since the cost functions may not converge using federated gradient aggregation in a minimax game between the discriminator and the generator. Several studies [4, 8, 31] have attempted to integrate the GAN-based framework with the federated learning. DP-FedAvg-GAN [4] trains GANs for image synthesis with differential privacy guarantees. In DP-FedAvg-GAN, the server holds a shared generator and discriminator that are delivered to clients. GS-WGAN [8] enables the release of a sanitized version of sensitive data while maintaining stringent privacy protections. GS-WGAN is capable of more precisely distorting gradient information, allowing for the training of deeper models that generate more informative samples. Federated CycleGAN [31] is specifically designed to perform the unsupervised image translation while maintaining data privacy.

### 3. Our FedMed-GAN

This section presents a detailed formulation of FedMed-GAN. We first briefly introduce the federated setting of FedMed-GAN. In Section 3.1, we illustrate how to set up the generators and discriminators in servers and clients (hospitals). Then we present distribution settings of unpaired multi-modal data among hospitals in Section 3.2. In Section 3.3, we demonstrate a privacy-preserving setting for FedMed-GAN, which is capable of generating high-dimensional data with a DP guarantee. In Section 3.4, we propose a novel edge loss to further improve the performance of our generator in FedMed-GAN with DP guarantee.

#### 3.1. Federated Model Setup

The federated setting of FedMed-GAN’s generator and discriminator is described in Fig. 2. We employ CycleGAN [37], MUNIT [14] and UNIT [24] as our baseline models. The task of FedMed-GAN is to generate a B-modal image by inputting an A-modal image.

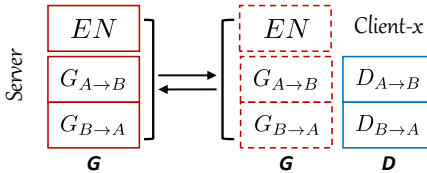


Figure 2. The federated setting of FedMed-GAN model.  $G$  denotes the shared generator and  $D$  denotes the discriminator.  $EN$  is the shared edge neural network.

CycleGAN [37] owns two generators and discriminators.  $EN$  is the edge feature extractor (edge-net).  $G_{A \rightarrow B}$  denotes that the role of the generator is to generate B-modal images from A-modal samples. While  $G_{B \rightarrow A}$  means that the role of the generator is to generate A-modal data from B-modal images.  $D_{A \rightarrow B}$  denotes that the role of the discriminator is to distinguish whether B-modal data generated from A-modal samples is fake.  $D_{B \rightarrow A}$  denotes that the role of the discriminator is to distinguish whether A-modal data generated from B-modal images is fake. The federated setting of CycleGAN is to locate two generators ( $G_{A \rightarrow B}$  and  $G_{B \rightarrow A}$ ) into the servers. It means that these two generators and edge-net of each hospital are aggregated into the server’s generators and edge-net. The server will also send its generators and edge-net into different hospitals after aggregation. The discriminators ( $D_{A \rightarrow B}$  and  $D_{B \rightarrow A}$ ) of each hospital are not shared with others. In MUNIT [14], there are two encoders ( $Enc_A$  and  $Enc_B$ ), two decoders ( $Dec_A$  and  $Dec_B$ ) and two discriminators ( $D_{A \rightarrow B}$  and  $D_{B \rightarrow A}$ ). The federated setting of MUNIT is to locate two encoders ( $Enc_A$  and  $Enc_B$ ) and decoders ( $Dec_A$  and  $Dec_B$ ) and edge-net  $EN$  into the server. However, the discriminators of each hospital are not shared with each other. In UNIT [24], there are two encoders ( $E_{A \rightarrow B}$  and  $E_{B \rightarrow A}$ ), two generators ( $G_{A \rightarrow B}$  and  $G_{B \rightarrow A}$ ) and two discriminators ( $D_{A \rightarrow B}$  and  $D_{B \rightarrow A}$ ). The federated setting of UNIT is to locate the encoders ( $E_{A \rightarrow B}$  and  $E_{B \rightarrow A}$ ), generators ( $G_{A \rightarrow B}$  and  $G_{B \rightarrow A}$ ) and edge-net ( $EN$ ) to the server. The federated settings of discriminators ( $D_{A \rightarrow B}$  and  $D_{B \rightarrow A}$ ) are the same as the ones in MUNIT.

The whole algorithm is described in Algorithm 1. The training algorithm for each client’s generator and edge network is written in Algorithm 2. The training algorithm for each client’s discriminator is written in Algorithm 3.

#### 3.2. Unsupervised Data Distribution Setting

Fig. 3 shows the distribution of multi-modal unpaired neural-imaging data settings. We assume that the multi-modal neural-imaging data allocated for each hospital are unpaired. For example, Hospital 1 owns 100 T1-weighted neural images and T2-weighted neural images, but all of them are unpaired. Moreover, various hospitals may own different numbers of unpaired data. For instance, we set the number of the hospital as 4. If we set the distribution method as average, the data proportion for each hospital as [0.25, 0.25, 0.25, 0.25]. If we set the distribution method as “extreme”, our data distribution meets the extreme long-tailed phenomenon, *i.e.*, the data proportion for each hospital could be [0.7, 0.1, 0.1, 0.1]. The experimental settings of our algorithm are detailed in Section 4.1 and Table 3.

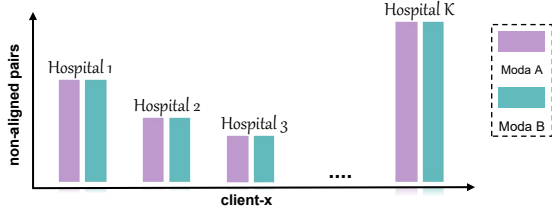


Figure 3. Multi-Modal Unpaired Data Distribution.

### 3.3. Differential Privacy

Fig. 4 shows the differential privacy mechanism of FedMed-GAN, which is inspired by DP-SGD [2] and GS-WGAN [8]. In order to stop privacy leakage from the server’s generators and edge-net, we train the client’s generators and edge-net ( $G_{A \rightarrow B}$ ,  $G_{B \rightarrow A}$ ,  $EN$  in Fig. 2) in a privacy-preserving manner. We adopt DP-SGD [2] as FedMed-GAN’s differential privacy method. DP-SGD enforces the differential privacy guarantees by clipping the gradient to bound sensitivity and adding calibrated random noise to introduce stochasticity. Specifically, only the generators ( $G_{A \rightarrow B}$  and  $G_{B \rightarrow A}$  in Fig. 4) and the edge-net ( $EN$  in Fig. 4) are released to the public. So we can only apply DP-SGD to the parameters  $\theta_G$  of generators and the parameters  $\theta_{EN}$  of edge-net:

$$g_G^t = \nabla_{\theta_G} \mathcal{L}_G(\theta_G^t, \theta_{EN}^t, \theta_D^t), \quad (1)$$

$$\hat{g}_G^t = M_{clip, \sigma} = clip(g^t, C) + \mathcal{N}(0, \sigma^2 C^2 I), \quad (2)$$

$$\theta_G^{t+1} = \theta_G^t - \eta_G \hat{g}_G^t, \quad (3)$$

$$g_E^t = \nabla_{\theta_{EN}} \mathcal{L}_{edge}(\theta_{EN}^t), \quad (4)$$

$$\hat{g}_E^t = M_{clip, \sigma} = clip(g_E^t, C) + \mathcal{N}(0, \sigma^2 C^2 I), \quad (5)$$

$$\theta_{EN}^{t+1} = \theta_{EN}^t - \eta_E \hat{g}_E^t, \quad (6)$$

where  $t$  is the epoch number in the training process.  $C$  denotes the clip bound of the gradient.  $\sigma$  represents the standard deviation of Gaussian noise.  $EN$  denotes the edge-net.  $g_G$  is the back-propagation gradient from the generator loss.  $g_E$  is the back-propagation gradient from the edge loss.  $\hat{g}_G$  is the clipped gradient after  $M_{clip, \sigma}$ . In Fig. 4(a), FedMed-GAN-CycleGAN is divided into two loops. One is to generate modality  $B'$  image from modality  $A$  image. The other loop is to generate modality  $A'$  image from modality  $B$  image. For example, Fig. 4(a)(1) shows the differential privacy mechanism of  $A \rightarrow B'$  loop. FedMed-GAN-CycleGAN applies DP-SGD mechanism  $M_{clip, \sigma}$  to the gradient  $g^{up}$  that is achieved from the back-propagation from the generator loss. The parameters of  $G_{A \rightarrow B}$  are updated by  $\hat{g}^{up}$ , which is the clipped gradients of  $g^{up}$ . The parameters of  $EN$  are updated by  $\hat{g}_E^{up}$ , which is clipped gradient of  $g_E^{up}$ . Fig. 4(b) shows that the differential privacy mechanism of FedMed-GAN-MUNIT. It is similar to Fig. 4(a). The difference is that the encoder and decoder are simultaneously

updated by the gradient  $\hat{g}^{up}$ .

### 3.4. Edge Loss

**Motivation** T2-weighted MRI and proton density weighting (PD) MRI highlight differences on modality-specific tissues. Proton density (PD) does not display the magnetic characteristics of the hydrogen nuclei but the number of nuclei in the area being imaged. However, we can see that PD and T2 have a similar edge feature map in Fig. 5. In other words, multi-modality MRI can hold the same or similar edge feature information. Moreover, if we can keep the edge information in the brain image synthesis process, it is of great help to the downstream segmentation task since segmentation task pays more attention to the edge detail. However, FedMed-GAN cannot preserve the edge information very well.

Fig. 5 shows the multi-modality neural image and their edge feature map of FedMedGAN-CycleGAN. In Fig. 5, A denotes PD and B denotes T2. The first row denotes the input domain-A image, while its feature map  $A_{edge}$ .  $A_{edge}$  shows the edge feature of modality A clearly.  $B'$  is generated from A and  $\hat{A}$  is generated from  $B'$ . In Fig. 5, the edge information of  $B'_{edge}$  and  $\hat{A}_{edge}$  are very blurred. So our motivation is to let the edge information  $A$ , *i.e.*,  $A_{edge}$ , guide the generation for modality  $B'$  image and the reconstructed modality  $\hat{A}$  image. The edge feature maps are extracted by RCF [26].

**Full Objective** As shown in Fig. 6, for each image in domain A, the image translation brings A back to the original image, *i.e.*,  $A \rightarrow B' \rightarrow \hat{A}$ . As we mentioned in the motivation of edge loss,  $B'$  and  $\hat{A}$  image should also have the same edge information as A :

$$A_{edge} \approx B'_{edge} \approx \hat{A}_{edge}. \quad (7)$$

In the loops of  $B \rightarrow A' \rightarrow \hat{B}$ , it also has:

$$B_{edge} \approx A'_{edge} \approx \hat{B}_{edge}. \quad (8)$$

So the edge loss of FedMed-GAN  $L_{edge}$  in loops  $A \rightarrow B' \rightarrow \hat{A}$  is:

$$L_{edge}(A \rightarrow B' \rightarrow \hat{A}) = \|A_{edge} - B'_{edge}\|_1 + \|B'_{edge} - \hat{A}_{edge}\|_1 + \|\hat{A}_{edge} - A_{edge}\|_1. \quad (9)$$

And the edge loss of FedMed-GAN  $L_{edge}$  in loops  $B \rightarrow A' \rightarrow \hat{B}$  is:

$$L_{edge}(B \rightarrow A' \rightarrow \hat{B}) = \|B_{edge} - A'_{edge}\|_1 + \|A'_{edge} - \hat{B}_{edge}\|_1 + \|\hat{B}_{edge} - B_{edge}\|_1. \quad (10)$$

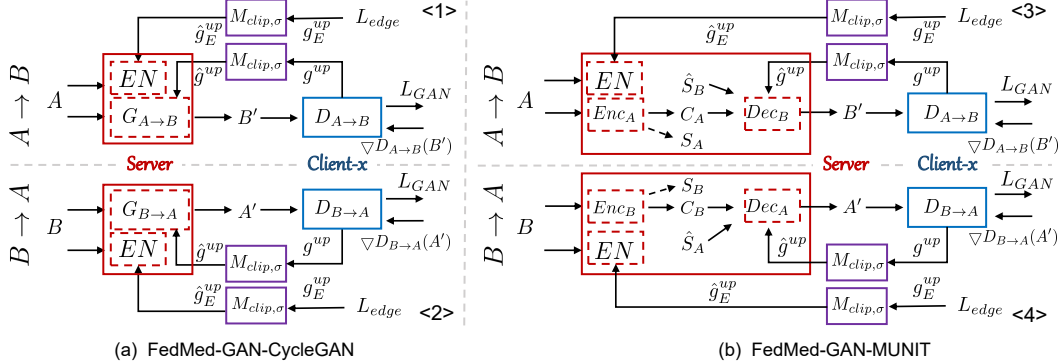


Figure 4. FedMed-GAN’s differential privacy settings.  $B'$  refers to the generated modality B image from modality A image.  $A'$  refers to the generated modality A image from modality B image.  $M_{\sigma, C}$  denotes DP-SGD’s operator.  $g_E$  is the back-propagation gradient from  $L_{edge}$ .  $\hat{g}_E$  denotes the clipped  $g_E$  after  $M_{clip, \sigma}$ .  $g^{up}$  denotes the  $g^{up}$  back-propagation gradient from discriminators to generators.  $\hat{g}^{up}$  denotes the clipped after  $M_{clip, \sigma}$ . The red part indicates the models are shared with servers and clients. The green part indicates the models are just located in the client and not shared with each other. Figure (a) refers to the differential privacy mechanism of FedMed-CycleGAN.  $G_{A \rightarrow B}$  and  $G_{B \rightarrow A}$  are the generators.  $D_{A \rightarrow B}$  and  $D_{B \rightarrow A}$  are the discriminators. Figure (b) refers to the differential privacy mechanism of FedMed-MUNIT.  $Enc_A$  and  $Enc_B$  are the encoders.  $C_A$  and  $S_A$  separately represent the content code and the style code of modality A image.  $C_B$  and  $S_B$  separately represent the content code and the style code of modality B image.  $\hat{S}_B$  denotes the style code of modality B image added with Gaussian Noise.  $\hat{S}_A$  denotes the style code of modality A image added with Gaussian Noise.

Simultaneously, we use  $L_{cycle}$  to avoid changing image pixels of intensity too much.

$$L_{cycle} = \|A - \hat{A}\|_1 + \|B - \hat{B}\|_1. \quad (11)$$

So the total edge loss for FedMed-GAN-CycleGAN:

$$\begin{aligned} L_{total} = & L_{GAN}(A \rightarrow B') + \\ & L_{GAN}(B \rightarrow A') + \\ & \lambda_1 L_{edge}(A \rightarrow B' \rightarrow \hat{A}) + \quad (12) \\ & \lambda_1 L_{edge}(B \rightarrow A' \rightarrow \hat{B}) + \\ & \lambda_2 L_{cycle}, \end{aligned}$$

where  $\lambda_1$  and  $\lambda_2$  are the weights of edge loss and cycle-consistency loss. The edge loss of FedMed-GAN-MUNIT is the same as the edge loss of FedMed-GAN-CycleGAN. Fig. 7 shows the detail of FedMed-GAN-MUNIT edge loss.

## 4. Experiments

### 4.1. Federated Data Setting

**IXI** [1] collects nearly 600 MR images from normal and healthy subjects at three hospitals. The MR image acquisition protocol for each subject includes T1, T2, PD-weighted images (PD), MRA images, and Diffusion-weighted images (15 directions). Here, we only use T1 (581 cases), T2 (578 cases), and PD (578 cases) data to conduct our experiments, and select the paired data with the same ID from the three modes. The image has a non-uniform length on the Z-axis with the size of 256 on the X-axis and Y-axis. The IXI data set is not divided into a training set and a test set. Therefore, we randomly split the whole data as the training set (0.8) and the test set (0.2).

### Algorithm 1: Server-orchestrated training loop

---

**Data:** total number of hospitals  $N \in \mathbb{N}$ , total number of rounds of  $T \in \mathbb{N}$ ,  $G(A \rightarrow B)$ :  $G_1, G(B \rightarrow A)$ :  $G_2, D(A \rightarrow B)$ :  $D_1, D(B \rightarrow A)$ :  $D_2$ , edge-net:  $EN$  and its parameters:  $\theta_{EN}$ , clients  $\theta_n$ , server  $\theta_S$

**Initialize:** generator  $\theta_{G1}^0$  and  $\theta_{G2}^0$ , discriminator  $\theta_{D1}^0$  and  $\theta_{D2}^0$ , EN:  $\theta_{EN}^0$

**for** each round  $t$  from 0 to  $T$  **do**

- for** each hospital  $n \in N$  in parallel **do**
- $\theta_{n:G1}^{t+1}, \theta_{n:G2}^{t+1}, \theta_{n:EN}^{t-1} \leftarrow$  ClientGenUpdate( $\theta_{G1}^t, \theta_{D1}^t, \theta_{G2}^t, \theta_{D2}^t$ )
- $\theta_{n:D1}^{t+1}, \theta_{n:D2}^{t+1} \leftarrow$  ClientDiscUpdate( $\theta_{D1}^t, \theta_{D2}^t$ )
- end**
- $\theta_{S:G1}^{t+1}, \theta_{S:G2}^{t+1}, \theta_{S:EN}^{t+1} \leftarrow$  Aggregate( $\theta_{n:G1}^{t+1}, \theta_{n:G2}^{t+1}, \theta_{n:EN}^{t+1}$ )
- end**

**Return:** Server generator  $\theta_{G1}$  and  $\theta_{G2}$

---

**BraTS2019** [30, 5] is constructed for analysis and diagnosis of brain disease. In the BraTS dataset, brain glioma is classified into the low-grade glioma (LGG) and the high-grade glioma (HGG). Two publicly available datasets of multi-institutional pre-operative MRI sequences are provided: training (HGG 259 cases and LGG 76 cases) and validation (125 cases). Each patient contributes  $155 \times 240 \times 240$  with four sequences: T1, T2, T1ce, and FLAIR.

**Data processing** If we consider the whole case, the data size is huge. To solve this problem, we split the three-dimensional volume and select slices from 50 to 80 on the Z-axis to ensure data validity and diversity. All of the im-

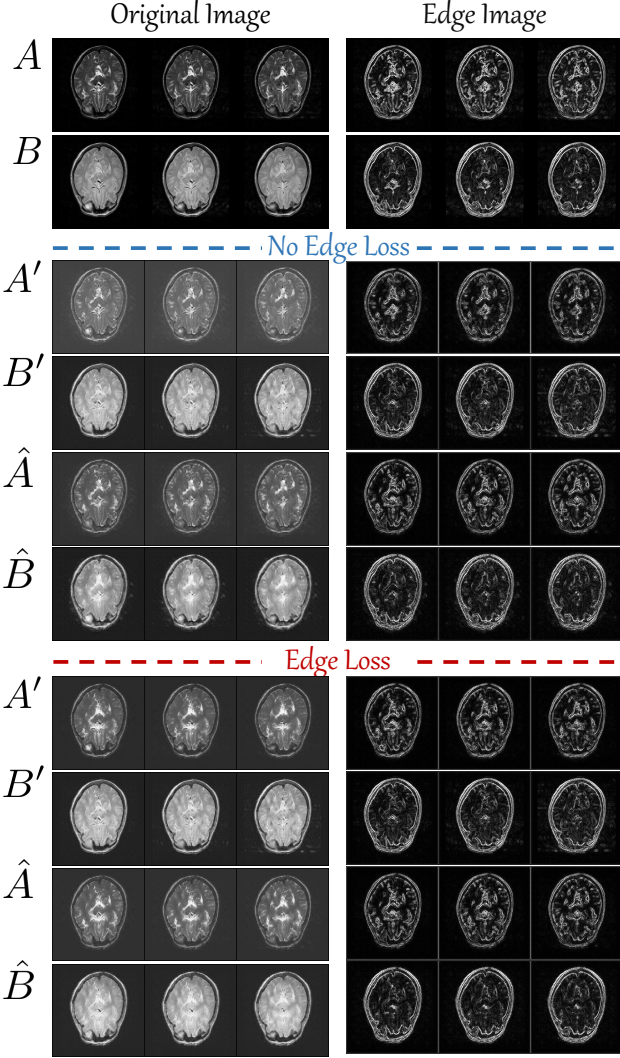


Figure 5. The multi-modality neural imaging data generated by FedMedGAN-CycleGAN and their edge map. The first row denotes the input domain-A image and its feature map  $A_{edge}$ .  $A_{edge}$  can clearly show the edge feature of modality  $A$ .  $B'$  is generated from  $A$  and  $\hat{A}$  is generated from  $B'$ . The second row denotes the input domain-B image and its feature map  $B_{edge}$ .  $A'$  is generated from  $B$  and  $\hat{B}$  is generated from  $A'$ .

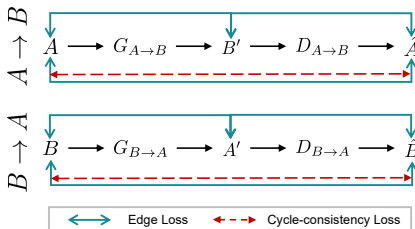


Figure 6. FedMed-GAN-CycleGAN Edge Loss and Cycle-consistency Loss.

ages of the two datasets are cropped into the size of 256

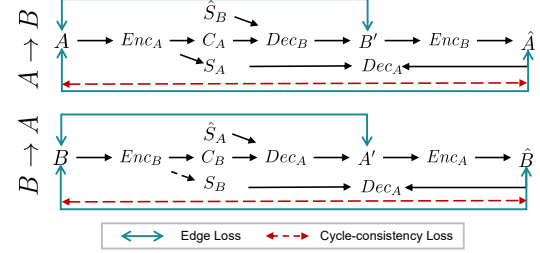


Figure 7. FedMed-GAN-MUNIT Edge Loss and Cycle-consistency loss.

**Algorithm 2:** ClientGenUpdate( $k, \theta_{D1}, \theta_{D2}, \theta_{G1}^0, \theta_{G2}^0, \theta_{EN}^0$ )

**Data:** total number of steps  $J \in \mathbb{N}$ , batch size  $S \in \mathbb{R}^+$ , learning rate  $\eta_G \in \mathbb{R}^+$ , gen. input size  $n_U \in \mathbb{N}$ ,  $A_{fake} = A', B_{fake} = B', G(A \rightarrow B): G_1$ ,  $G(B \rightarrow A): G_2$ ,  $\hat{A} = G_2(B')$ ,  $\hat{B} = G_1(A')$ , clip bound  $C$ , noise standard deviation  $\sigma$ , gradient sensitization mechanism  $\mathcal{M}$ ,

**Loss function:**  $L_{G1}(\theta_{G1}, \theta_{D1}; B')$ ,  $L_{G2}(\theta_{G2}, \theta_{D2}; A')$ ,  $L_{edge} = L_{edge}(A \rightarrow B' \rightarrow \hat{A}) + L_{edge}(B \rightarrow A' \rightarrow \hat{B})$ ,  $L_{cycle}(A, \hat{A}, B, \hat{B})$

**Initialize:**  $\theta_{G1} \leftarrow \theta_{G1}^0, \theta_{G2} \leftarrow \theta_{G2}^0, \theta_{EN} \leftarrow \theta_{EN}^0, s \leftarrow k$ 's unpaired data split into  $S$  batches

**for** each generator training step  $j$  from 1 to  $J$  **do**

$U_A \leftarrow$  (sample  $S$  random vectors of dim.  $n_U$ )

$U_B \leftarrow$  (sample  $S$  random vectors of dim.  $n_U$ )

$A' \leftarrow G(U_B, \theta_G)$

$B' \leftarrow G(U_A, \theta_G)$

$g_1 = \nabla(\mathcal{L}(\theta_{G1}; B', \theta_{D1}) + \mathcal{L}_{edge} + \mathcal{L}_{cycle})$

$g_2 = \nabla(\mathcal{L}(\theta_{G2}; A', \theta_{D2}) + \mathcal{L}_{edge} + \mathcal{L}_{cycle})$

$g_E = \nabla \mathcal{L}_{edge}$

$\hat{g}_1 = \mathcal{M}(g_1) = \text{clip}(g_1, C) + N(\sigma^2 C^2 I)$

$\hat{g}_2 = \mathcal{M}(g_2) = \text{clip}(g_2, C) + N(\sigma^2 C^2 I)$

$\hat{g}_E = \mathcal{M}(g_E) = \text{clip}(g_E, C) + N(\sigma^2 C^2 I)$

$\theta_{G1} = \theta_{G1} - \eta_G \hat{g}_1$

$\theta_{G2} = \theta_{G2} - \eta_G \hat{g}_2$

$\theta_{EN} = \theta_{EN} - \eta_E \hat{g}_E$

**end**

**Return:** client generator  $\theta_{G1}, \theta_{G2}$  and edge-net  $\theta_{EN}$

pixels. After that, we randomly select two subjects with different IDs and randomly select slices of them with the same ID from different modalities to construct our unpaired data. Finally, we select 6,000 unpaired images as our training data to achieve the unsupervised scheme.

**Metrics** We employ three metrics to evaluate our generator's performance. The first is mean absolute error (MAE):

$$MAE = \frac{1}{nm} \sum_{n=1}^{i=1} \sum_{m=1}^{j=1} |T_{ij} - G_{ij}|, \quad (13)$$

where  $T_{ij}$  denotes the ground truth neuroimage pixel and  $G_{ij}$  denotes the generated neuroimage pixel. The lower value of MAE means the better performance.

---

**Algorithm 3:** ClientDiscUpdate( $k, \theta_{G1}, \theta_{G2}, \theta_{D1}^0, \theta_{D2}^0$ )

---

**Data:** number of steps  $J \in \mathbb{N}$ , batch size  $S \in \mathbb{R}^+$ , learning rate  $\eta_G \in \mathbb{R}^+$ , gen. input size  $n_U \in \mathbb{N}$ ,  $A_{fake} = A'$ ,  $B_{fake} = B'$ ,  $G(A \rightarrow B)$ :  $G_1$ ,  $G(B \rightarrow A)$ :  $G_2$ ,  $D(A \rightarrow B)$ :  $D_1$ ,  $D(B \rightarrow A)$ :  $D_2$

**Loss function:**  $L_{D1}(\theta_{D1}; B, B')$ , loss function  $L_{D2}(\theta_{D2}; A, A')$

**Initialize:**  $\theta_{D1} \leftarrow \theta_{D1}^0, \theta_{D2} \leftarrow \theta_{D2}^0, s \leftarrow k$ 's unpaired data split into  $S$  batches

**for** each generator training step  $j$  from 1 to  $J$  **do**

$U_A \leftarrow$  (sample  $S$  random vectors of dim.  $n_U$ )

$U_B \leftarrow$  (sample  $S$  random vectors of dim.  $n_U$ )

$B' \leftarrow G_1(U_A, \theta_{G1})$

$A' \leftarrow G_2(U_B, \theta_{G2})$

$\theta_{D1} = \theta_{D1} - \eta_D \bigtriangledown (L(\theta_{D1}; B, B'))$

$\theta_{D2} = \theta_{D2} - \eta_D \bigtriangledown (L(\theta_{D2}; A, A'))$

**end**

**Return:** client generator  $\theta_{D1}$  and  $\theta_{D2}$

---

The second metric is the peak signal-to-noise ratio (PSNR). PSNR is a function of the mean squared error and better to evaluate the context (edge) detail of neuroimages. The higher PSNR value means the better performance.

$$PSNR = -10 \log_{10} \left( \frac{1}{nm} \sum_n^{i=1} \sum_m^{j=1} (T_{ij} - G_{ij})^2 \right) \quad (14)$$

The third metric is structural similarity index (SSIM), which is a weighted combination of the luminance, the contrast and the structure. The higher SSIM value means the better performance.

$$SSIM = \frac{(2\mu_T\mu_G + C_1)(2\sigma_{TG} + C_2)}{(\mu_T^2 + \mu_G^2 + C_1)(\sigma_T^2 + \sigma_G^2 + C_2)} \quad (15)$$

The  $\mu$  and  $\sigma$  in SSIM are the mean value and standard deviation of an image, respectively.  $C_1$  and  $C_2$  are two positive constants. We set  $C_1$  and  $C_2$  are 0.01 and 0.03, respectively.

**Implementations** We use the learning rate of  $1e-4$  and the batch size of 8. For the centralized training method, the number of the epoch is set to 10. For each round of federated training, each client is trained for 3 epochs. The optimizer is Adam [19]. Its beta1 and beta2 are 0.5 and 0.999, respectively. The edge network structure is RCF [26]. The edge feature map of neuroimaging data is the last fusion image in RCF [26]. The weights of GAN loss, Edge loss and Cycle loss are 1.0, 10.0, 1.0, respectively.

**Baseline Setting and Results** We build up FedMedGAN Benchmarks for the BraTS2019 dataset [30, 5] and the IXI dataset [1] in Table 1 and Table 2, respectively. The baseline models are CycleGAN [37], MUNIT [14] and UNIT [24]. In BraTS, we leverage [T1, T2, FLAIR] modality MRI. In IXI, we utilize [PD, T2] modality data. For our

federated setting, the client number is 4 for the baseline results. The data distribution proportion for the clients is [0.4, 0.3, 0.2, 0.1]. The number of communication round is set to 10. The aggregation method is Fed-Avg [27]. In terms of differential privacy setting, the Gaussian noise  $\mu$  is set to 1.07 and the standard deviation  $\sigma$  is set to 2.0. The clip bound for back-propagation gradient is set to 1.0. Note that due to the page limitation, we put the experiments of the BraTS2019 dataset into the Supplementary Material.

## 4.2. Edge Loss Ablation Study

**Multiple Rounds** Fig. 8 shows ablation studies of multiple communication rounds on the IXI dataset. We adopt two aggregation strategies: Fed-Avg [27] and Fed-PSNR-Best. The Fed-Avg method aggregates the weight from each client's generator model and edge network to the server model according to the data proportion distribution for each client. The Fed-PSNR-Best method adopts the best client generator model and edge neural network as the server model for each round and sends them to each client.

In Fig. 8 (a), the federated training strategy is Fed-Avg. From the 3rd epoch (1st round), the edge loss significantly increases the server performance and speeds up the convergence rate. Furthermore, the edge loss can stabilize the generator training process and does not sacrifice the performance compared with the centralized training (Non-Fed) method. We can obtain the same conclusion when aggregation strategy is changed to Fed-PSNR-Best, seen in Fig. 8 (b). In addition, Fig. 8 (c) clearly shows that centralized training (Non-Fed) for medical GAN may meet the generator mode collapse issue. But our edge loss can both increases the convergent rate of the server generator model and solve the generator mode collapse issue.

**Multiple Clients and Data Distribution** Table 3 shows that our edge loss can help the performance of FedMedGAN with better stability or even superior when facing with data long-tailed phenomenon. In Table 3, our data distribution method is divided into ['average', 'gradual', 'extreme']. For instance, when the client number is 4 and proportion is  $0.7+0.1\times 3$  (extreme mode), it means that the original total data assign 70% to the first client and assign 10% to the other three clients. The baseline model is FedMed-GAN-CycleGAN. The aggregation strategy is Fed-Avg. The task of Table 3 is to generate PD-weighted MRI from T2-weighted MRI.

**Various Gradient Clip Bound and Noise Range** Table 4 shows that the edge loss could mitigate the performance drop due to the differential privacy guarantee. In Table 4, the baseline model is FedMed-GAN-CycleGAN. The task is to generate the PD-weighted data from the T2-weighted inputs. In FedMed-GAN differential privacy settings, the level of gradient clip bound is classified into [0.7, 1.0, 1.3]. The noise is divided into [0.5, 1.07, 2.0]. From

Table 1. Baseline results on the BraTS2019 dataset.

|          | Method   | Indicator | T1 → T2 | T1 → FLAIR | T2 → T1 | T2 → FLAIR | FLAIR → T1 | FLAIR → T2 |
|----------|----------|-----------|---------|------------|---------|------------|------------|------------|
| Non-Fed. | MUNIT    | MAE       | 0.0452  | 0.0492     | 0.0466  | 0.0459     | 0.0382     | 0.0420     |
|          |          | PSNR      | 21.743  | 19.818     | 20.123  | 20.141     | 21.623     | 21.721     |
|          |          | SSIM      | 0.8980  | 0.8853     | 0.9371  | 0.9023     | 0.9543     | 0.9117     |
|          | UNIT     | MAE       | 0.0437  | 0.0507     | 0.0536  | 0.0487     | 0.0482     | 0.0410     |
|          |          | PSNR      | 20.833  | 20.190     | 20.067  | 20.266     | 20.493     | 21.212     |
|          |          | SSIM      | 0.8855  | 0.8936     | 0.9313  | 0.8930     | 0.9338     | 0.9101     |
|          | CycleGAN | MAE       | 0.0567  | 0.0535     | 0.0557  | 0.0462     | 0.0471     | 0.0454     |
|          |          | PSNR      | 19.244  | 20.098     | 19.012  | 20.683     | 20.315     | 20.979     |
|          |          | SSIM      | 0.8427  | 0.8984     | 0.9192  | 0.9140     | 0.9371     | 0.9003     |
| Fed.     | MUNIT    | MAE       | 0.0783  | 0.0934     | 0.0972  | 0.0960     | 0.1031     | 0.0782     |
|          |          | PSNR      | 16.653  | 15.377     | 15.724  | 15.275     | 14.931     | 17.048     |
|          |          | SSIM      | 0.6850  | 0.6463     | 0.8325  | 0.6402     | 0.8048     | 0.7114     |
|          | UNIT     | MAE       | 0.2631  | 0.2458     | 0.3461  | 0.2331     | 0.3443     | 0.3150     |
|          |          | PSNR      | 9.3403  | 9.5427     | 7.9660  | 10.284     | 7.4321     | 7.6504     |
|          |          | SSIM      | 0.0563  | 0.2066     | 0.0359  | 0.1768     | 0.0187     | 0.0555     |
|          | CycleGAN | MAE       | 0.0609  | 0.0565     | 0.0565  | 0.0508     | 0.0470     | 0.0591     |
|          |          | PSNR      | 18.506  | 18.620     | 18.620  | 19.904     | 20.540     | 19.402     |
|          |          | SSIM      | 0.8507  | 0.9146     | 0.9146  | 0.8954     | 0.9405     | 0.8666     |

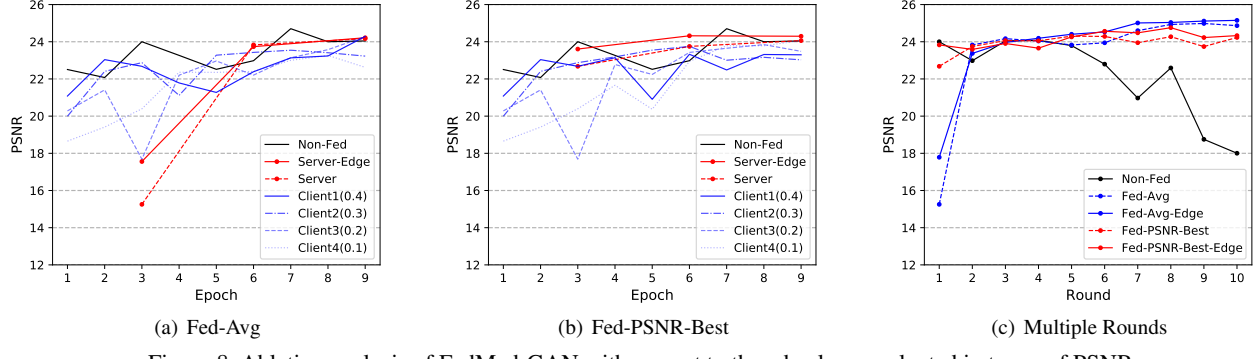


Figure 8. Ablation analysis of FedMed-GAN with respect to the edge loss, evaluated in terms of PSNR.

Table 2. Baseline results on the IXI dataset.

|          | Method   | Indicator | T2 → PD | PD → T2 |
|----------|----------|-----------|---------|---------|
| Non-Fed. | MUNIT    | MAE       | 0.0366  | 0.0324  |
|          |          | PSNR      | 23.498  | 23.994  |
|          |          | SSIM      | 0.9666  | 0.9524  |
|          | UNIT     | MAE       | 0.0417  | 0.0356  |
|          |          | PSNR      | 22.671  | 23.000  |
|          |          | SSIM      | 0.9575  | 0.9380  |
|          | CycleGAN | MAE       | 0.0356  | 0.0315  |
|          |          | PSNR      | 24.702  | 24.145  |
|          |          | SSIM      | 0.9715  | 0.9516  |
| Fed.     | MUNIT    | MAE       | 0.1093  | 0.0842  |
|          |          | PSNR      | 16.263  | 17.057  |
|          |          | SSIM      | 0.8393  | 0.7033  |
|          | UNIT     | MAE       | 0.9800  | 0.2570  |
|          |          | PSNR      | 9.4781  | 8.8979  |
|          |          | SSIM      | 0.1587  | 0.0471  |
|          | CycleGAN | MAE       | 0.0401  | 0.0364  |
|          |          | PSNR      | 24.061  | 23.824  |
|          |          | SSIM      | 0.9666  | 0.9472  |

Table 4, the edge loss can increase the server's generator performance with various differential privacy guarantees.

Table 3. Multiple clients and different data distributions in terms of Edge-Loss on the IXI dataset.

| Scheme  | Client Num. | 2         | 4                     | 8                              |
|---------|-------------|-----------|-----------------------|--------------------------------|
| Average | Proportion  | 0.5 × 2   | 0.25 × 4              | 0.125 × 8                      |
|         | MAE         | 0.0443    | 0.0396                | 0.0396                         |
|         | PSNR        | 23.628    | 23.831                | 23.914                         |
|         | SSIM        | 0.9642    | 0.9663                | 0.9664                         |
| Gradual | Proportion  | 0.6 + 0.4 | 0.4 + 0.3 + 0.2 + 0.1 | 0.3 + 0.2 + 0.1 × 4 + 0.05 × 2 |
|         | MAE         | 0.0398    | 0.0401                | 0.0433                         |
|         | PSNR        | 23.878    | 24.061                | 23.624                         |
|         | SSIM        | 0.9663    | 0.9666                | 0.9627                         |
| Extreme | Proportion  | 0.9 + 0.1 | 0.7 + 0.1 × 3         | 0.6 + 0.1 × 7                  |
|         | MAE         | 0.0454    | 0.0392                | 0.0421                         |
|         | PSNR        | 24.084    | 23.722                | 23.899                         |
|         | SSIM        | 0.9636    | 0.9649                | 0.9673                         |

## 5. Conclusions

We build up a new federated multi-modal brain image synthesize (FedMed-GAN) benchmark. Furthermore, we propose a novel edge-loss to speed up FedMed-GAN's con-

Table 4. Noise comparisons using Edge Loss on the IXI dataset.

| No-Edge / Edge | Clip-bound (0.7)              | Clip-bound (1.0)       | Clip-bound (1.3)       |
|----------------|-------------------------------|------------------------|------------------------|
| Noise (0.5)    | MAE ↓ 0.0402 / <b>0.3560</b>  | 0.0400 / 0.0405        | 0.0379 / 0.0408        |
|                | PSNR ↑ 24.020 / <b>24.662</b> | 23.545 / <b>23.992</b> | 24.114 / 24.106        |
|                | SSIM ↑ 0.9668 / <b>0.9710</b> | 0.9645 / <b>0.9679</b> | 0.9676 / 0.9670        |
| Noise (1.07)   | MAE ↓ 0.0393 / 0.0431         | 0.0401 / <b>0.0372</b> | 0.0402 / <b>0.0378</b> |
|                | PSNR ↑ 23.910 / <b>24.066</b> | 24.061 / <b>24.321</b> | 23.718 / <b>24.281</b> |
|                | SSIM ↑ 0.9656 / <b>0.9676</b> | 0.9666 / <b>0.9694</b> | 0.9647 / <b>0.9686</b> |
| Noise (2.0)    | MAE ↓ 0.0453 / <b>0.0348</b>  | 0.0412 / <b>0.0358</b> | 0.0409 / <b>0.0378</b> |
|                | PSNR ↑ 23.140 / <b>24.740</b> | 23.903 / <b>24.504</b> | 23.384 / <b>24.184</b> |
|                | SSIM ↑ 0.9597 / <b>0.9719</b> | 0.9641 / <b>0.9700</b> | 0.9629 / <b>0.9681</b> |

verge rate and reduce the performance gap brought by differential privacy. In addition, our novel edge-guided training paradigm can help to bridge the performance gap between the centralized learning and the federated learning. We believe that this benchmark can significantly promote this research field into both medical image community and federated learning community.

**Potential Negative Societal Impact** FedMed-GAN can facilitate medical GAN since paired neuroimaging data are expensive or difficult to collect. However, a potential negative factor is to generate fake examples for some unsuitable applications by leveraging edge-guided FedMed-GAN.

## References

- [1] Ixi dataset. <https://brain-development.org/ixi-dataset/>.
- [2] Martin Abadi, Andy Chu, Ian Goodfellow, H Brendan McMahan, Ilya Mironov, Kunal Talwar, and Li Zhang. Deep learning with differential privacy. In *Proceedings of the 2016 ACM SIGSAC conference on computer and communications security*, pages 308–318, 2016.
- [3] Sean Augenstein, H Brendan McMahan, Daniel Ramage, Swaroop Ramaswamy, Peter Kairouz, Mingqing Chen, Rajiv Mathews, et al. Generative models for effective ml on private, decentralized datasets. *arXiv preprint arXiv:1911.06679*, 2019.
- [4] Sean Augenstein, H. Brendan McMahan, Daniel Ramage, Swaroop Ramaswamy, Peter Kairouz, Mingqing Chen, Rajiv Mathews, and Blaise Agüera y Arcas. Generative models for effective ML on private, decentralized datasets. In *ICLR*. OpenReview.net, 2020.
- [5] Spyridon Bakas, Hugo J. Kuijf, Bjoern H. Menze, and Mauricio Reyes. Brainlesion: Glioma, multiple sclerosis, stroke and traumatic brain injuries. In *Lecture Notes in Computer Science*, 2017.
- [6] Guha Balakrishnan, Amy Zhao, Mert R. Sabuncu, John V. Gutttag, and Adrian V. Dalca. Voxelmorph: A learning framework for deformable medical image registration. *IEEE Trans. Medical Imaging*, 38(8):1788–1800, 2019.
- [7] Dingfan Chen, Tribhuvanesh Orekondy, and Mario Fritz. Gswgan: A gradient-sanitized approach for learning differentially private generators. *arXiv preprint arXiv:2006.08265*, 2020.
- [8] Dingfan Chen, Tribhuvanesh Orekondy, and Mario Fritz. GS-WGAN: A gradient-sanitized approach for learning differentially private generators. In *NeurIPS*, 2020.
- [9] Runfa Chen, Wenbing Huang, Binghui Huang, Fuchun Sun, and Bin Fang. Reusing discriminators for encoding: Towards unsupervised image-to-image translation. In *CVPR*, pages 8165–8174. Computer Vision Foundation / IEEE, 2020.
- [10] Adrian V. Dalca, Guha Balakrishnan, John V. Gutttag, and Mert R. Sabuncu. Unsupervised learning of probabilistic diffeomorphic registration for images and surfaces. *Medical Image Anal.*, 57:226–236, 2019.
- [11] Adrian V. Dalca, Marianne Rakic, John V. Gutttag, and Mert R. Sabuncu. Learning conditional deformable templates with convolutional networks. In *NeurIPS*, pages 804–816, 2019.
- [12] Ian Goodfellow, Jean Pouget-Abadie, Mehdi Mirza, Bing Xu, David Warde-Farley, Sherjil Ozair, Aaron Courville, and Yoshua Bengio. Generative adversarial nets. *Advances in neural information processing systems*, 27, 2014.
- [13] Xun Huang, Ming-Yu Liu, Serge J. Belongie, and Jan Kautz. Multimodal unsupervised image-to-image translation. In *ECCV(3)*, volume 11207 of *Lecture Notes in Computer Science*, pages 179–196. Springer, 2018.
- [14] Xun Huang, Ming-Yu Liu, Serge Belongie, and Jan Kautz. Multimodal unsupervised image-to-image translation. In *Proceedings of the European conference on computer vision (ECCV)*, pages 172–189, 2018.
- [15] Yawen Huang, Ling Shao, and Alejandro F. Frangi. DOTE: dual convolutional filter learning for super-resolution and cross-modality synthesis in MRI. In *MICCAI (3)*, volume 10435 of *Lecture Notes in Computer Science*, pages 89–98. Springer, 2017.
- [16] Yawen Huang, Feng Zheng, Runmin Cong, Weilin Huang, Matthew R. Scott, and Ling Shao. MCMT-GAN: multi-task coherent modality transferable GAN for 3d brain image synthesis. *IEEE Trans. Image Process.*, 29:8187–8198, 2020.
- [17] Yawen Huang, Feng Zheng, Danyang Wang, Weilin Huang, Matthew R. Scott, and Ling Shao. Brain image synthesis with unsupervised multivariate canonical cscl4net. In *CVPR*, pages 5881–5890. Computer Vision Foundation / IEEE, 2021.
- [18] Phillip Isola, Jun-Yan Zhu, Tinghui Zhou, and Alexei A. Efros. Image-to-image translation with conditional adversarial networks. In *CVPR*, pages 5967–5976. IEEE Computer Society, 2017.
- [19] Diederik P Kingma and Jimmy Ba. Adam: A method for stochastic optimization. *arXiv preprint arXiv:1412.6980*, 2014.
- [20] Lingke Kong, Chenyu Lian, Detian Huang, Zhenjiang Li, Yanle Hu, and Qichao Zhou. Breaking the dilemma of medical image-to-image translation, 2021.
- [21] Hsin-Ying Lee, Hung-Yu Tseng, Jia-Bin Huang, Maneesh Singh, and Ming-Hsuan Yang. Diverse image-to-image translation via disentangled representations. In *ECCV (1)*, volume 11205 of *Lecture Notes in Computer Science*, pages 36–52. Springer, 2018.
- [22] Hsin-Ying Lee, Hung-Yu Tseng, Qi Mao, Jia-Bin Huang, Yu-Ding Lu, Maneesh Singh, and Ming-Hsuan Yang.

DRIT++: diverse image-to-image translation via disentangled representations. *Int. J. Comput. Vis.*, 128(10):2402–2417, 2020.

[23] Tian Li, Anit Kumar Sahu, Manzil Zaheer, Maziar Sanjabi, Ameet Talwalkar, and Virginia Smith. Federated optimization in heterogeneous networks. In *MLSys*. mlsys.org, 2020.

[24] Ming-Yu Liu, Thomas M. Breuel, and Jan Kautz. Unsupervised image-to-image translation networks. In *NIPS*, pages 700–708, 2017.

[25] Ming-Yu Liu, Xun Huang, Arun Mallya, Tero Karras, Timo Aila, Jaakko Lehtinen, and Jan Kautz. Few-shot unsupervised image-to-image translation. In *ICCV*, pages 10550–10559. IEEE, 2019.

[26] Yun Liu, Ming-Ming Cheng, Xiaowei Hu, Kai Wang, and Xiang Bai. Richer convolutional features for edge detection. In *Proceedings of the IEEE conference on computer vision and pattern recognition*, pages 3000–3009, 2017.

[27] Brendan McMahan, Eider Moore, Daniel Ramage, Seth Hampson, and Blaise Agüera y Arcas. Communication-efficient learning of deep networks from decentralized data. In *Artificial intelligence and statistics*, pages 1273–1282. PMLR, 2017.

[28] Brendan McMahan, Eider Moore, Daniel Ramage, Seth Hampson, and Blaise Agüera y Arcas. Communication-efficient learning of deep networks from decentralized data. In *AISTATS*, volume 54 of *Proceedings of Machine Learning Research*, pages 1273–1282. PMLR, 2017.

[29] Olaf Ronneberger, Philipp Fischer, and Thomas Brox. U-net: Convolutional networks for biomedical image segmentation. In *MICCAI (3)*, volume 9351 of *Lecture Notes in Computer Science*, pages 234–241. Springer, 2015.

[30] Rebecca L. Siegel, Kimberly D Miller, and Ahmedin Jemal. Cancer statistics, 2019. *CA: A Cancer Journal for Clinicians*, 69, 2019.

[31] Joonyoung Song and Jong Chul Ye. Federated cyclegan for privacy-preserving image-to-image translation. *CoRR*, abs/2106.09246, 2021.

[32] Hongyi Wang, Mikhail Yurochkin, Yuekai Sun, Dimitris S. Papailiopoulos, and Yasaman Khazaeni. Federated learning with matched averaging. In *ICLR*. OpenReview.net, 2020.

[33] Mikhail Yurochkin, Mayank Agarwal, Soumya Ghosh, Kristjan H. Greenewald, Trong Nghia Hoang, and Yasaman Khazaeni. Bayesian nonparametric federated learning of neural networks. In *ICML*, volume 97 of *Proceedings of Machine Learning Research*, pages 7252–7261. PMLR, 2019.

[34] Sixiao Zheng, Jiachen Lu, Hengshuang Zhao, Xiatian Zhu, Zekun Luo, Yabiao Wang, Yanwei Fu, Jianfeng Feng, Tao Xiang, Philip H. S. Torr, and Li Zhang. Rethinking semantic segmentation from a sequence-to-sequence perspective with transformers. In *CVPR*, pages 6881–6890. Computer Vision Foundation / IEEE, 2021.

[35] Yi Zhou, Xiaodong He, Shanshan Cui, Fan Zhu, Li Liu, and Ling Shao. High-resolution diabetic retinopathy image synthesis manipulated by grading and lesions. In *MICCAI (1)*, volume 11764 of *Lecture Notes in Computer Science*, pages 505–513. Springer, 2019.

[36] Zongwei Zhou, Md Mahfuzur Rahman Siddiquee, Nima Tajbakhsh, and Jianming Liang. Unet++: A nested u-net architecture for medical image segmentation. In *DLMIA/MLCDS@MICCAI*, volume 11045 of *Lecture Notes in Computer Science*, pages 3–11. Springer, 2018.

[37] Jun-Yan Zhu, Taesung Park, Phillip Isola, and Alexei A Efros. Unpaired image-to-image translation using cycle-consistent adversarial networks. In *Proceedings of the IEEE international conference on computer vision*, pages 2223–2232, 2017.

# FedMed-GAN Supplementary Materials

Guoyang Xie<sup>1,2,†</sup>, Jinbao Wang<sup>2,5,†</sup>, Yawen Huang<sup>3,†</sup>, Yefeng Zheng<sup>3</sup>, Feng Zheng<sup>2</sup>, Jingkuang Song<sup>5</sup>,  
Yaochu Jin<sup>1,4</sup>

<sup>1</sup>NICE Group, University of Surrey

<sup>2</sup>VIP Lab, Southern University of Science and Technology

<sup>3</sup>Javis Lab, Tencent

<sup>4</sup>Bielefeld University

<sup>5</sup>University of Electronic Science and Technology of China  
 {guoyang.xie, yaochu.jin}@surrey.ac.uk,  
 {wangjb, zhengf}@sustech.edu.cn,  
 {yawenhuang, yefeng.zheng}@tencent.com,  
 jingkuan.song@gmail.com

In this supplementary materials, we first provide ablation studies of multiple clients with different data distributions in Section 1, then explore the performance of various gradient clip bound and noise settings in Section 2, and finally give visualization results of our proposed FedMed-GAN in Section 3.

**Implementations:** Here, we have conducted a series of experiments with limited computing resources and hence use a unified experimental setup. The baseline model is FedMed-GAN-CycleGAN [?] with the Fed-Avg [?] aggregation strategy. We use the learning rate of  $1e-4$  and the batch size of 8. For the centralized training method, the number of the epoch is set to 10. For each round of federated training, each client is trained for 3 epochs. The optimizer is Adam [?]. Its beta1 and beta2 are 0.5 and 0.999, respectively. The edge network structure is RCF [?]. The edge feature map of neuroimaging data is the last fusion image in RCF [?]. The weights of GAN loss, edge loss, and cycle loss are 1.0, 10.0, 1.0, respectively.

## 1. Multiple clients and data distributions

Tables of 1-8 provide detailed baseline results without edge loss on the IXI dataset [?] and the BraTS2019 dataset [?]. From the experimental results, we can see that our proposed FedMed-GAN can achieve good results with different data distributions and multiple clients. Even when the data volume of each client is very small, *i.e.*  $0.125 \times 8$ , the performance of our edge-guided FedMed-GAN does not deteriorate.

Meanwhile, Tables of 1-4 also list the results with edge

loss for more comprehensive analysis. From the comparisons, we can conclude that our proposed edge-guide FedMed-GAN can improve performance effectively.

## 2. Various gradient clip bound and noise range

Tables of 9-12 present our baseline results of FedMed-GAN with different clip bounds and noise intensities. From the results, we can see that the performance of our edge-guided FedMed-GAN is stable in different noise settings. Moreover, we observe that the edge loss could help FedMed-GAN to achieve better performance on the IXI dataset and the BraTS2019 dataset.

## 3. Visualization

We visualize several cases of multi-modality images generated by our FedMed-GAN as shown in Fig. 1, Fig. 2, Fig. 3 and Fig. 4. We observe that Fig. 1 and Fig. 2 produce clear results on the IXI dataset, indicating that our model works well. However, since the input image quality is poor or corrupted caused by tumors, *i.e.* the BraTS dataset, it degrades the performance of the generators, as shown in Fig. 3 and Fig. 4. Therefore, the input image quality plays an important role in the medical image generation task. In the future, we will focus on enhancing the domain generalization ability for the corrupted neuroimaging data.

<sup>†</sup>Equal contribution.

Table 1. FedMed-GAN-CycleGAN (PD → T2) on IXI.

| Scheme  | Client Num. | 2               | 4                       | 8  |
|---------|-------------|-----------------|-------------------------|--|
| Average | Proportion  | $0.5 \times 2$  | $0.25 \times 4$         | $0.125 \times 8$                           |
|         | MAE         | 0.0307 / 0.0332 | 0.0319 / 0.0418         | 0.0422 / 0.0416                            |
|         | PSNR        | 24.313 / 23.890 | 23.759 / 22.129         | 21.750 / 21.610                            |
|         | SSIM        | 0.9543 / 0.9480 | 0.9430 / 0.9045         | 0.9049 / 0.9058                            |
| Gradual | Proportion  | $0.6 + 0.4$     | $0.4 + 0.3 + 0.2 + 0.1$ | $0.3 + 0.2 + 0.1 \times 4 + 0.05 \times 2$ |
|         | MAE         | 0.0313 / 0.0313 | 0.0340 / 0.0323         | 0.0348 / 0.0326                            |
|         | PSNR        | 24.186 / 24.111 | 24.177 / 23.845         | 23.830 / 23.555                            |
|         | SSIM        | 0.9476 / 0.9492 | 0.9495 / 0.9422         | 0.9456 / 0.9414                            |
| Extreme | Proportion  | $0.9 + 0.1$     | $0.7 + 0.1 \times 3$    | $0.6 + 0.1 \times 7$                       |
|         | MAE         | 0.0340 / 0.0341 | 0.0312 / 0.0302         | 0.0440 / 0.0470                            |
|         | PSNR        | 24.038 / 23.902 | 24.437 / 24.594         | 21.770 / 22.169                            |
|         | SSIM        | 0.9490 / 0.9500 | 0.9547 / 0.9554         | 0.9190 / 0.9319                            |

Table 2. FedMed-GAN-CycleGAN (T2 → T1) on BraTS2019.

| Scheme  | Client Num. | 2                | 4                       | 8  |
|---------|-------------|------------------|-------------------------|--|
| Average | Proportion  | $0.5 \times 2$   | $0.25 \times 4$         | $0.125 \times 8$                           |
|         | MAE         | 0.0551 / 0.0639  | 0.0531 / 0.0549         | 0.0589 / 0.0558                            |
|         | PSNR        | 18.645 / 18.026  | 18.876 / 18.619         | 18.454 / 18.666                            |
|         | SSIM        | 0.9126 / 0.8986  | 0.9163 / 0.9087         | 0.9091 / 0.9110                            |
| Gradual | Proportion  | $0.6 + 0.4$      | $0.4 + 0.3 + 0.2 + 0.1$ | $0.3 + 0.2 + 0.1 \times 4 + 0.05 \times 2$ |
|         | MAE         | 0.0629 / 0.0550  | 0.0535 / 0.0572         | 0.0633 / 0.0597                            |
|         | PSNR        | 17.998 / 18.744  | 19.008 / 18.444         | 18.113 / 18.294                            |
|         | SSIM        | 0.9063 / 0.9167  | 0.9172 / 0.9034         | 0.9042 / 0.9033                            |
| Extreme | Proportion  | $0.9 + 0.1$      | $0.7 + 0.1 \times 3$    | $0.6 + 0.1 \times 7$                       |
|         | MAE         | 0.0574 / 0.0516  | 0.0552 / 0.0612         | 0.0629 / 0.0717                            |
|         | PSNR        | 18.7879 / 19.648 | 18.839 / 18.715         | 18.468 / 17.395                            |
|         | SSIM        | 0.9187 / 0.9293  | 0.9086 / 0.9073         | 0.9152 / 0.8958                            |

Table 3. FedMed-GAN-CycleGAN (T1 → FLAIR) on BraTS2019.

| Scheme  | Client Num. | 2               | 4                       | 8  |
|---------|-------------|-----------------|-------------------------|--|
| Average | Proportion  | $0.5 \times 2$  | $0.25 \times 4$         | $0.125 \times 8$                           |
|         | MAE         | 0.0483 / 0.0475 | 0.0523 / 0.0503         | 0.0589 / 0.0534                            |
|         | PSNR        | 20.116 / 20.236 | 19.763 / 20.167         | 19.746 / 20.089                            |
|         | SSIM        | 0.8946 / 0.9123 | 0.8711 / 0.8897         | 0.8895 / 0.9042                            |
| Gradual | Proportion  | $0.6 + 0.4$     | $0.4 + 0.3 + 0.2 + 0.1$ | $0.3 + 0.2 + 0.1 \times 4 + 0.05 \times 2$ |
|         | MAE         | 0.0608 / 0.0594 | 0.0518 / 0.0510         | 0.0513 / 0.0492                            |
|         | PSNR        | 18.846 / 19.213 | 19.351 / 19.879         | 20.100 / 20.782                            |
|         | SSIM        | 0.8231 / 0.8342 | 0.8710 / 0.0892         | 0.9001 / 0.8954                            |
| Extreme | Proportion  | $0.9 + 0.1$     | $0.7 + 0.1 \times 3$    | $0.6 + 0.1 \times 7$                       |
|         | MAE         | 0.0537 / 0.512  | 0.0517 / 0.0523         | 0.0564 / 0.0502                            |
|         | PSNR        | 19.748 / 20.856 | 20.405 / 20.623         | 20.204 / 20.869                            |
|         | SSIM        | 0.8935 / 0.9241 | 0.9034 / 0.9175         | 0.9051 / 0.9132                            |

Table 4. FedMed-GAN-CycleGAN (T2 → FLAIR) on BraTS2019.

| Scheme  | Client Num. | 2               | 4                       | 8  |
|---------|-------------|-----------------|-------------------------|--|
| Average | Proportion  | $0.5 \times 2$  | $0.25 \times 4$         | $0.125 \times 8$                           |
|         | MAE         | 0.0399 / 0.0387 | 0.0466 / 0.0433         | 0.0504 / 0.0485                            |
|         | PSNR        | 23.888 / 23.946 | 20.374 / 20.456         | 19.838 / 20.120                            |
|         | SSIM        | 0.9663 / 0.9554 | 0.9074 / 0.9234         | 0.8961 / 0.9121                            |
| Gradual | Proportion  | $0.6 + 0.4$     | $0.4 + 0.3 + 0.2 + 0.1$ | $0.3 + 0.2 + 0.1 \times 4 + 0.05 \times 2$ |
|         | MAE         | 0.0501 / 0.0492 | 0.0466 / 0.456          | 0.0512 / 0.0489                            |
|         | PSNR        | 20.399 / 20.867 | 20.374 / 20.467         | 20.054 / 20.450                            |
|         | SSIM        | 0.8951 / 0.9125 | 0.9074 / 0.9134         | 0.8912 / 0.9013                            |
| Extreme | Proportion  | $0.9 + 0.1$     | $0.7 + 0.1 \times 3$    | $0.6 + 0.1 \times 7$                       |
|         | MAE         | 0.0463 / 0.0512 | 0.0495 / 0.0480         | 0.0505 / 0.0496                            |
|         | PSNR        | 20.363 / 19.982 | 20.380 / 20.432         | 19.784 / 19.526                            |
|         | SSIM        | 0.9078 / 0.9179 | 0.9007 / 0.9132         | 0.8965 / 0.8732                            |

Table 5. FedMed-GAN-CycleGAN (T2 → PD) on IXI.

| Scheme  | Client Num. | 2              | 4                       | 8  |
|---------|-------------|----------------|-------------------------|--|
| Average | Proportion  | $0.5 \times 2$ | $0.25 \times 4$         | $0.125 \times 8$                           |
|         | MAE         | 0.0399         | 0.0389                  | 0.0429                                     |
|         | PSNR        | 23.892         | 23.620                  | 22.633                                     |
|         | SSIM        | 0.9646         | 0.9643                  | 0.9576                                     |
| Gradual | Proportion  | $0.6 + 0.4$    | $0.4 + 0.3 + 0.2 + 0.1$ | $0.3 + 0.2 + 0.1 \times 4 + 0.05 \times 2$ |
|         | MAE         | 0.0369         | 0.0434                  | 0.0485                                     |
|         | PSNR        | 24.238         | 23.776                  | 23.597                                     |
|         | SSIM        | 0.9676         | 0.9639                  | 0.9623                                     |
| Extreme | Proportion  | $0.9 + 0.1$    | $0.7 + 0.1 \times 3$    | $0.6 + 0.1 \times 7$                       |
|         | MAE         | 0.0424         | 0.0378                  | 0.0600                                     |
|         | PSNR        | 23.568         | 24.303                  | 21.138                                     |
|         | SSIM        | 0.9638         | 0.9686                  | 0.9413                                     |

Table 6. FedMed-GAN-CycleGAN (T1 → T2) on BraTS2019.

| Scheme  | Client Num. | 2              | 4                       | 8  |
|---------|-------------|----------------|-------------------------|--|
| Average | Proportion  | $0.5 \times 2$ | $0.25 \times 4$         | $0.125 \times 8$                           |
|         | MAE         | 0.0545         | 0.0514                  | 0.0596                                     |
|         | PSNR        | 18.626         | 18.821                  | 18.832                                     |
|         | SSIM        | 0.8595         | 0.8396                  | 0.8497                                     |
| Gradual | Proportion  | $0.6 + 0.4$    | $0.4 + 0.3 + 0.2 + 0.1$ | $0.3 + 0.2 + 0.1 \times 4 + 0.05 \times 2$ |
|         | MAE         | 0.0499         | 0.0546                  | 0.0574                                     |
|         | PSNR        | 19.414         | 18.993                  | 19.025                                     |
|         | SSIM        | 0.8688         | 0.8563                  | 0.8566                                     |
| Extreme | Proportion  | $0.9 + 0.1$    | $0.7 + 0.1 \times 3$    | $0.6 + 0.1 \times 7$                       |
|         | MAE         | 0.0582         | 0.0517                  | 0.0678                                     |
|         | PSNR        | 19.046         | 18.875                  | 18.035                                     |
|         | SSIM        | 0.8690         | 0.8444                  | 0.8443                                     |

Table 7. FedMed-GAN-CycleGAN (FLAIR → T1) on BraTS2019.

| Scheme  | Client Num. | 2              | 4                       | 8  |
|---------|-------------|----------------|-------------------------|--|
| Average | Proportion  | $0.5 \times 2$ | $0.25 \times 4$         | $0.125 \times 8$                           |
|         | MAE         | 0.0499         | 0.0484                  | 0.0536                                     |
|         | PSNR        | 19.787         | 20.265                  | 19.996                                     |
|         | SSIM        | 0.9316         | 0.9348                  | 0.9311                                     |
| Gradual | Proportion  | $0.6 + 0.4$    | $0.4 + 0.3 + 0.2 + 0.1$ | $0.3 + 0.2 + 0.1 \times 4 + 0.05 \times 2$ |
|         | MAE         | 0.0477         | 0.0493                  | 0.0549                                     |
|         | PSNR        | 20.372         | 20.113                  | 20.151                                     |
|         | SSIM        | 0.9354         | 0.9316                  | 0.9342                                     |
| Extreme | Proportion  | $0.9 + 0.1$    | $0.7 + 0.1 \times 3$    | $0.6 + 0.1 \times 7$                       |
|         | MAE         | 0.0488         | 0.0508                  | 0.0549                                     |
|         | PSNR        | 20.522         | 20.610                  | 19.938                                     |
|         | SSIM        | 0.9376         | 0.9360                  | 0.9321                                     |

Table 8. FedMed-GAN-CycleGAN (FLAIR → T2) on BraTS2019.

| Scheme  | Client Num. | 2              | 4                       | 8  |
|---------|-------------|----------------|-------------------------|--|
| Average | Proportion  | $0.5 \times 2$ | $0.25 \times 4$         | $0.125 \times 8$                           |
|         | MAE         | 0.0417         | 0.0470                  | 0.0561                                     |
|         | PSNR        | 21.071         | 19.740                  | 20.273                                     |
|         | SSIM        | 0.9028         | 0.8630                  | 0.9311                                     |
| Gradual | Proportion  | $0.6 + 0.4$    | $0.4 + 0.3 + 0.2 + 0.1$ | $0.3 + 0.2 + 0.1 \times 4 + 0.05 \times 2$ |
|         | MAE         | 0.0454         | 0.0456                  | 0.0433                                     |
|         | PSNR        | 20.476         | 20.113                  | 20.453                                     |
|         | SSIM        | 0.8985         | 0.8709                  | 0.8898                                     |
| Extreme | Proportion  | $0.9 + 0.1$    | $0.7 + 0.1 \times 3$    | $0.6 + 0.1 \times 7$                       |
|         | MAE         | 0.0402         | 0.0403                  | 0.0551                                     |
|         | PSNR        | 21.149         | 21.302                  | 20.1884                                    |
|         | SSIM        | 0.9081         | 0.9003                  | 0.8928                                     |

Table 9. FedMed-GAN-CycleGAN (PD → T2) on IXI.

| No-Edge / Edge  | Clip-bound<br>(0.7) | Clip-bound<br>(1.0) | Clip-bound<br>(1.3) |
|-----------------|---------------------|---------------------|---------------------|
| Noise<br>(0.5)  | MAE                 | 0.0341 / 0.0338     | 0.0308 / 0.0309     |
|                 | PSNR                | 23.587 / 23.659     | 24.081 / 23.971     |
|                 | SSIM                | 0.9386 / 0.9391     | 0.9504 / 0.9484     |
| Noise<br>(1.07) | MAE                 | 0.0396 / 0.0358     | 0.0378 / 0.0323     |
|                 | PSNR                | 23.687 / 23.848     | 23.359 / 23.845     |
|                 | SSIM                | 0.9353 / 0.9453     | 0.9353 / 0.9422     |
| Noise<br>(2.0)  | MAE                 | 0.0310 / 0.0319     | 0.0362 / 0.0325     |
|                 | PSNR                | 24.031 / 24.165     | 23.116 / 23.888     |
|                 | SSIM                | 0.9468 / 0.9510     | 0.9265 / 0.9458     |

Table 10. FedMed-GAN-CycleGAN (T2 → PD) on IXI.

| No-Edge / Edge  | Clip-bound<br>(0.7) | Clip-bound<br>(1.0) | Clip-bound<br>(1.3) |
|-----------------|---------------------|---------------------|---------------------|
| Noise<br>(0.5)  | MAE                 | 0.0402 / 0.0399     | 0.0391 / 0.0396     |
|                 | PSNR                | 24.115 / 23.888     | 23.678 / 23.895     |
|                 | SSIM                | 0.9663 / 0.9663     | 0.9653 / 0.9658     |
| Noise<br>(1.07) | MAE                 | 0.0509 / 0.0395     | 0.0414 / 0.0394     |
|                 | PSNR                | 23.201 / 23.919     | 23.811 / 23.964     |
|                 | SSIM                | 0.9596 / 0.9667     | 0.9644 / 0.9658     |
| Noise<br>(2.0)  | MAE                 | 0.0387 / 0.0409     | 0.0450 / 0.0362     |
|                 | PSNR                | 23.892 / 23.736     | 23.917 / 24.413     |
|                 | SSIM                | 0.9660 / 0.9634     | 0.9660 / 0.9692     |

Table 11. FedMed-GAN-CycleGAN (T1 → T2) on BraTS2019.

| No-Edge / Edge  | Clip-bound<br>(0.7) | Clip-bound<br>(1.0) | Clip-bound<br>(1.3) |
|-----------------|---------------------|---------------------|---------------------|
| Noise<br>(0.5)  | MAE                 | 0.0503 / 0.0520     | 0.0528 / 0.0512     |
|                 | PSNR                | 19.048 / 18.967     | 18.700 / 19.004     |
|                 | SSIM                | 0.8445 / 0.8595     | 0.8432 / 0.8561     |
| Noise<br>(1.07) | MAE                 | 0.0518 / 0.0660     | 0.0512 / 0.0519     |
|                 | PSNR                | 18.830 / 18.761     | 18.985 / 18.711     |
|                 | SSIM                | 0.8401 / 0.8438     | 0.8590 / 0.8442     |
| Noise<br>(2.0)  | MAE                 | 0.0531 / 0.0555     | 0.0566 / 0.0518     |
|                 | PSNR                | 19.027 / 18.689     | 18.652 / 18.766     |
|                 | SSIM                | 0.8538 / 0.8358     | 0.8397 / 0.8494     |

Table 12. FedMed-GAN-CycleGAN (T2 → T1) on BraTS2019.

| No-Edge / Edge  | Clip-bound<br>(0.7) | Clip-bound<br>(1.0) | Clip-bound<br>(1.3) |
|-----------------|---------------------|---------------------|---------------------|
| Noise<br>(0.5)  | MAE                 | 0.0563 / 0.0544     | 0.0608 / 0.0570     |
|                 | PSNR                | 18.740 / 18.767     | 18.339 / 18.489     |
|                 | SSIM                | 0.9046 / 0.9138     | 0.9081 / 0.9139     |
| Noise<br>(1.07) | MAE                 | 0.0606 / 0.0552     | 0.0600 / 0.0572     |
|                 | PSNR                | 18.502 / 18.615     | 18.290 / 18.444     |
|                 | SSIM                | 0.9084 / 0.9110     | 0.9050 / 0.9034     |
| Noise<br>(2.0)  | MAE                 | 0.0590 / 0.0566     | 0.0600 / 0.0586     |
|                 | PSNR                | 18.129 / 18.599     | 18.105 / 18.413     |
|                 | SSIM                | 0.9009 / 0.9073     | 0.9018 / 0.0899     |

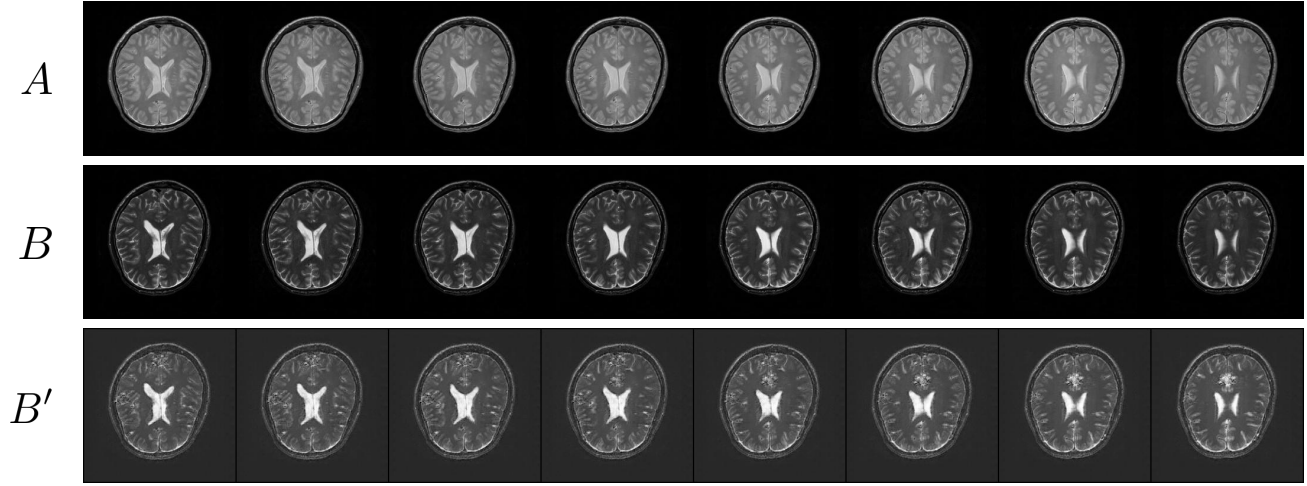


Figure 1. The multi-modality neural imaging data generated by FedMedGAN-CycleGAN on the IXI dataset, where  $A$ ,  $B$  and  $B'$  are input real PD image, the real T2-weighted image, and the T2-weighted image generated by real PD image, respectively.

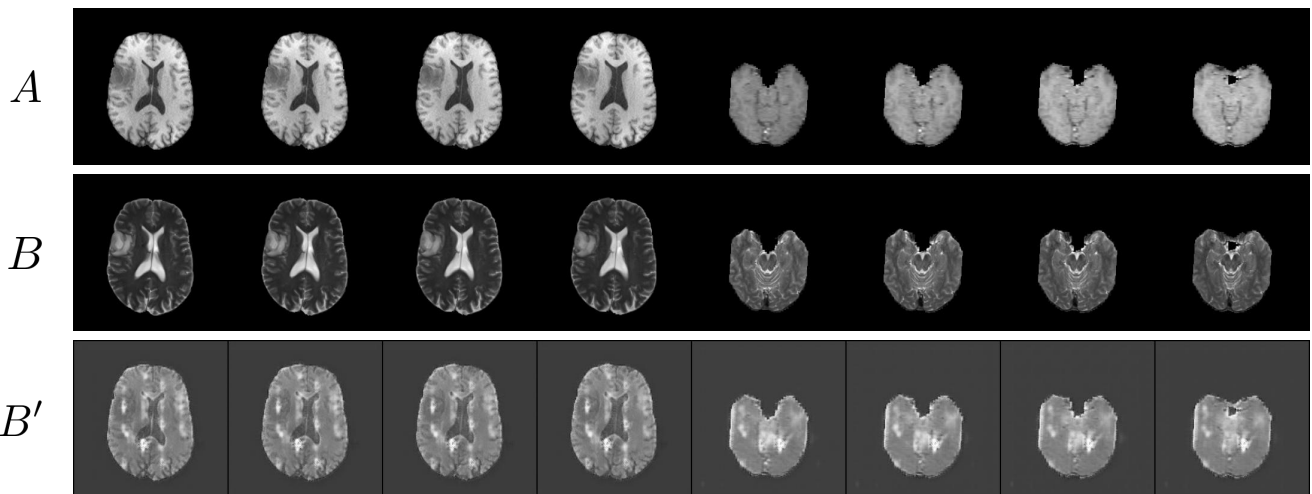


Figure 2. The multi-modality neural imaging data generated by FedMedGAN-CycleGAN on the BraTS2019 dataset, where  $A$ ,  $B$  and  $B'$  are real T1-weighted image, the real T2-weighted image, and the T2-weighted image generated by T1-weighted image, respectively.

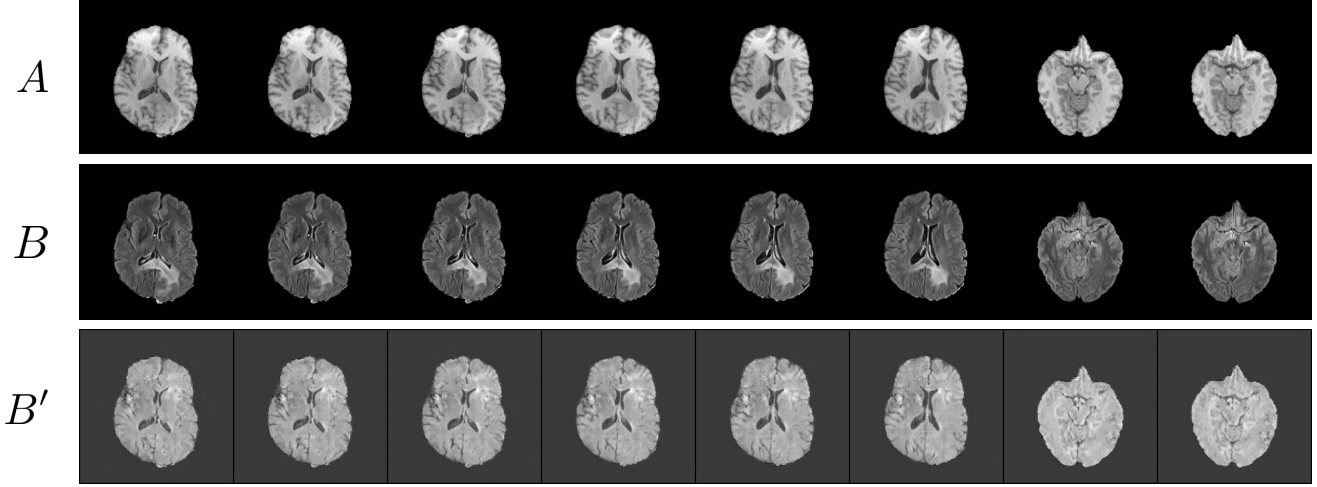


Figure 3. The multi-modality neural imaging data generated by FedMedGAN-CycleGAN on the BraTS2019 dataset, where  $A$ ,  $B$  and  $B'$  are the real T1-weighted image, the real FLAIR image, and the FLAIR image generated by T1-weighted image, respectively.

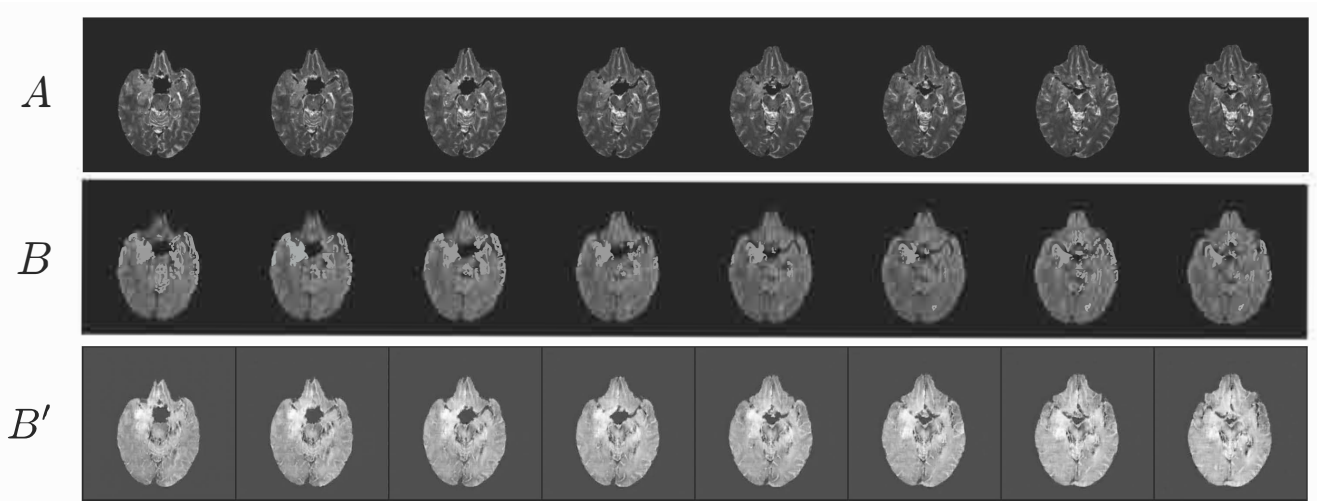


Figure 4. The multi-modality neural imaging data generated by FedMedGAN-CycleGAN on the BraTS2019 dataset, where  $A$ ,  $B$  and  $B'$  are input real T2 modal image, the real FLAIR modal image, and the output FLAIR modal image, respectively.